Endothelial Prohibitin Mediates Bidirectional Long-Chain Fatty Acid Transport in White and Brown Adipose Tissues

Zhanguo Gao, Alexes C. Daquinag, Yongmei Yu, and Mikhail G. Kolonin

Diabetes 2022;71:1400–1409 | https://doi.org/10.2337/db21-0972

The function of prohibitin-1 (PHB1) in adipocyte mitochondrial respiration, adaptive thermogenesis, and long-chain fatty acid (LCFA) metabolism has been reported. While intracellular PHB1 expression is ubiquitous, cell surface PHB1 localization is selective for adipocytes and endothelial cells of adipose tissue. The importance of PHB1 in adipose endothelium has not been investigated, and its vascular cell surface function has remained unclear. Here, we generated and analyzed mice with PHB1 knock-out specifically in endothelial cells (PHB1 EC-KO). Despite the lack of endothelial PHB1, mice developed normally and had normal vascularization in both white adipose tissue and brown adipose tissue (BAT). Tumor and ex vivo explant angiogenesis assays also have not detected a functional defect in PHB1 KO endothelium. No metabolic phenotype was observed in PHB1 EC-KO mice raised on a regular diet. We show that both male and female PHB1 EC-KO mice have normal body composition and adaptive thermogenesis. However, PHB1 EC-KO mice displayed higher insulin sensitivity and increased glucose clearance when fed a high-fat diet. We demonstrate that the efficacy of LCFA deposition by adipocytes is decreased by PHB1 EC-KO, in particular in BAT. Consistent with that, EC-KO mice have a defect in clearing triglycerides from systemic circulation. Free fatty acid release upon lipolysis induction was also found to be reduced in PHB1 EC-KO mice. Our results demonstrate that PHB1 in endothelial cells regulates bidirectional LCFA transport and thereby suppresses glucose utilization.

Prohibitin-1 (PHB1) is a ubiquitously expressed multifunctional protein (1). Genetic and pharmacological PHB1 targeting studies have identified the diverse functions of this protein in various organs and pathologies (2). Multifaceted functions of PHB1 have surfaced and turned out to be particularly important in adipose tissue (AT) (3). The ability of adipocytes to store and metabolize lipids predetermines susceptibility to metabolic diseases. White AT (WAT), presented as visceral AT (VAT) and subcutaneous AT (SAT), stores lipids (4). While excessive lipid accumulation of WAT adipocytes is linked with type 2 diabetes (T2D) (5), adipocytes of brown AT (BAT) and beige adipocytes in SAT can also expend energy through adaptive thermogenesis (6).

Cell type-specific roles of PHB1 are in part explained by its distinct functions in different cellular compartments. It has been shown that mitochondrial PHB1 is important for normal function of adipocytes in AT (3,7). However, recent studies have indicated a separate role of cell surface-localized PHB1 in AT (8). A peptide sequence KGGRAKD, binding to PHB1, has revealed PHB1 expression on the surface of endothelium selectively in AT (9). In search for PHB1 function in WAT, we have identified annexin A2 (ANX2) as a PHB1-binding protein containing a domain mimicked by the WAT-homing peptide KGGRAKD (8,10). We have shown that ANX2 and PHB1 are found in a protein complex present in the cell membrane lipid rafts of both mouse and human WAT (10). We subsequently demonstrated that PHB1 and ANX2 are found in a complex with the fatty acid translocase CD36 and demonstrated that the PHB1 supports CD36-mediated long-chain fatty acid (LCFA) uptake by adipocytes in cell culture (8). Recently, we reported that mice lacking adipocyte PHB1 are diabetic due to a defect in mitochondrial respiration and uncoupling/thermogenesis in brown adipocytes (7). However, this study also demonstrated that PHB1 contributes to LCFA

The Brown Foundation Institute of Molecular Medicine, University of Texas Health Science Center, Houston, TX

Corresponding author: Mikhail G. Kolonin, mikhail.g.kolonin@uth.tmc.edu

Received 29 October 2021 and accepted 27 March 2022

This article contains supplementary material online at https://doi.org/10.2337/figshare.19566058.

transport in adipocytes. The relative importance of cell surface-localized and intracellular PHB1 in AT endothelium has remained unclear.

Here, we generated and analyzed mice with PHB1 knockout (KO) specifically in endothelial cells (ECs). We demonstrate that PHB1 is dispensable for angiogenesis and that it modulates metabolism by promoting bidirectional LCFA transport though ECs.

RESEARCH DESIGN AND METHODS

Animal Experiments

All animal experimentations were approved by the University of Texas Health Animal Care and Use Committee. Mice were housed in the animal facility with a 12-h light/dark cycle at a temperature of 22–24°C, with free access to water and diet. PHB1 fl/fl (11) and TIE2e-Cre (12) mice were used for generating KO mice. PCR genotyping was performed as previously described (7,13). For diet-inducted obesity induction, mice were fed a 58 kcal% (fat) diet (Research Diets, D12331). For tumor studies, 1×10^5 cancer cells were grafted with a 21-gauge needle into the mammary fat pad (E0771) or subcutaneously onto the upper flank (RM1), as described (13). Body composition was measured using EchoMRI-100T (Echo Medical Systems). Indirect calorimetry studies were performed with OXYMAX (Columbus Instruments) Comprehensive Lab Animal Monitoring System (CLAMS), as described previously (14). Food intake and spontaneous locomotor activity were quantified over a 2-day time course at the same time. The core body temperature was determined using a MicroTherma 2 K High Precision Type K Thermocouple Meter (THS-221-092, ThermoWorks)/RET-3 rectal probe (Braintree Scientific), as described (14). Cold tolerance/adaptive thermogenesis was measured upon placing mice into an environmental chamber IS33SD (Powers Scientific), as described (14). For glucose tolerance test (GTT), glucose (2 g/kg body wt) was injected i.p. into overnight-fasted mice. For insulin tolerance test (ITT), insulin (0.6 units/kg body wt) was injected i.p. into mice fasted for 4 h. Blood glucose concentration was measured with a glucometer (One Touch Ultra). Intravenous (iv) lipid tolerance tests were performed by injecting overnight-fasted mice with 100 μL of 20% Intralipid LCFA emulsion. Blood from the tail vein was measured for triglycerides (TAG) using the EnzyChrom Triglyceride Assay Kit (BioAssay System, cat no. ETGA-200). Lipolysis was induced by i.p. injection of isoproterenol (10 mg/kg). Plasma free fatty acids (FFAs) were measured with the EnzyChrom Free Fatty Assay Kit (BioAssay System, cat no. EFFA-100). For radiolabeled LCFA biodistribution analysis (13), 6 μCi of [9,10-^{3}H(N)]-palmitic acid (NET043001MC; PerkinElmer, Waltham, MA) was injected iv. Its tissue uptake was measured by liquid scintillation counting by using Wallac 1209 RackBeta (LKB), as described (15,16). BODIPY-C_{16} (Molecular Probes, Waltham, MA) was injected iv (0.1 mg).

Cell and Tissue Analysis

Paraformaldehyde-fixed cells and formalin-fixed paraffin-embedded tissue sections were analyzed by immunofluorescence (IF), as described previously (7,13). Upon blocking, primary (4°C for 12 h) and secondary (room temperature for 1 h) antibody incubations were performed. Anti-PHB1 (1:100; Invitrogen, cat no. MA5-32000), antiperilipin1 (1:200; Abcam, cat no. ab61682), antiendomucin (1:100; R&D, cat no. AF4666), and anti-ANX2 (1:75; R&D, cat no. AF3928) antibodies, as well as secondary donkey Alexa 488-conjugated (1:200) and Cy3-conjugated (1:300) IgG from Jackson ImmunoResearch, were diluted in PBS with 0.05% Tween 20. Biotinylated isolectin B4 (1:50; Vector B-1205) binding was detected with Alexa-488– or Dylight-650–labeled streptavidin (Invitrogen, Carlsbad, CA), as described (7,13). Nuclei were stained with Hoechst 33258 (Invitrogen, H3569). Images were acquired with a confocal Leica TCS SP5 microscope/LAS AF software (Leica), or Carl Zeiss upright Apotome Axio Imager Z1/ZEN2 Core Imaging software. ImageJ analysis software was used to quantify data.

Cell Isolation and Cell Culture Assays

For adipocyte and stromal/vascular fraction (SVF) cell isolation, SAT pads of 8-week-old mice were excised, minced, and digested in 0.5 mg/mL collagenase type I (Worthington Biochemical, cat no. LS004196) and 2.5 mg/mL of Dispase (Roche, cat no. 04942078001) solution in a shaking bath for 1 h at 37°C. The cell suspension was filtered through a 70-μm cell strainer (Thomas Scientific, cat no. 1181X53), followed by centrifugation at 360*g* for 5 min at room temperature. Pelleted cells were plated in DMEM/10% FBS. The AT explant angiogenic sprouting assay was performed, as previously described (8,17). To construct pLenti-CRISPR/Cas9 PHB1 guide RNA expression vector, target sequence 5′-TGGAAAGTTCGGCCTGGCGTTGG-3′ containing the PAM sequence (underlined) was ligated into Lenti-CRISPR v2 plasmid (no. 52961, Addgene, Watertown, MA). For transendothelial transport assay, bEND.3 (wild-type [WT] and PHB1 KO) cells were grown to 100% confluency on top of the 0.4-μm pore transwells; adipocytes differentiated from WT mouse embryo fibroblasts (MEFs) were seeded in the bottom of the wells. BODIPY-C_{16} (2 μmol/L) was added to the upper chamber, and then adipocytes in the lower chamber were imaged after times indicated.

Statistical Analysis

All statistical analyses were performed with GraphPad Prism 6 software. Experimental results are shown as mean ± SEM. Two-tailed Student unpaired *t* tests were performed to compare littermates, unless otherwise indicated. $P < 0.05$ was considered significant.

Data and Resource Availability

Additional data and critical resources supporting the reported findings, methods, and conclusions will be available upon request.

RESULTS

Mice With Endothelial Deletion of PHB1 Have Normal AT and Vascularization

To create a model with a KO of PHB1 in ECs, we used the TIE2e-Cre mouse strain with endothelial- specific Cre expression (12). We crossed these mice with $PHB1^{fl/fl}$ strain (11) in which the *PHB1* gene is flanked by loxP recombination sites. The resulting TIE2e-Cre; $PHB1^{fl/fl}$ (EC-KO) and control Cre-negative $PHB1^{fl/fl}$ (WT) littermates were identified by PCR genotyping (Supplementary Fig. 1*A*). PHB1 KO was confirmed by IF on the cells of WAT SVF cells plated in culture. Isolectin B4 (IB4), binding to ECs (apparent as large and cobblestone colony-forming cells) and monocytes (apparent as small individual cells), was used as a marker. In KO SVF, no PHB1 protein was observed in ECs, while stromal cells were PHB1-positive, as expected (Fig. 1*A*). As expected, PHB1 expression was observed in adipocytes differentiated from MEFs of EC-KO mice (Supplementary Fig. 1*B*). EC-specific loss of PHB1 expression was also evident from IF analysis of SAT, in which ECs were identified by endomucin IF (Fig. 1*B*). Four-color IF with IB4 as an EC marker confirmed these findings for VAT (Fig. 1*C* and *D*) as well as for SAT and BAT (Supplementary Fig. 1*C*). The PHB1 signal was specifically lost in $IB4^{+}$ blood vessels while present in adipocytes and other nonendothelial cells of EC-KO mice, which was quantified by ImageJ software (Fig. 1*C*).

There was no difference detected in AT organization and adipocyte size between PHB1 EC-KO and WT littermates. Specifically, we extensively analyzed the vasculature for possible abnormalities. No differences were detected in VAT, SAT, or BAT vasculature organization between WT and PHB1-KO mice (Fig. 1*D* and Supplementary Fig. 1*C*). This indicated that endothelial PHB1 is not required for vascular development. WAT explants, established as described previously (8,17), also did not reveal a significant difference in endothelial sprouting between WT and PHB1 KO (Fig. 1*E*). We also investigated the role of endothelial PHB1 by using the tumor angiogenesis model in vivo. RM1 prostate carcinoma (Fig. 1*F*) and EO771 breast carcinoma (Supplementary Fig. 1*D*) grafts grew at least as large in KO mice as in WT mice. No defect in neovascularization was observed in sections of PHB1-KO tumors (Fig. 1*G*). VAT blood vessel density was also comparable for WT and EC-KO mice fed the high-fat diet (HFD), which promotes AT expansion accompanied by angiogenesis (Fig. 1*G*). These data indicate that PHB1 is dispensable for endothelial cell proliferation and sprouting. Interestingly, while cancer cells in both WT and EC-KO mice expressed PHB1 as expected (Fig. 1*F*), there was an apparent difference in their physiology. In KO mice, cancer cells had reduced expression of hydroxyacyl-CoA dehydrogenase (HADHA), the enzyme catalyzing the last three steps of mitochondrial fatty acid oxidation (FAO) (18), suggesting a decrease in β-oxidation (Supplementary Fig. 1*E*). To determine whether tumors instead switch to glucose utilization, we measured the expression of GLUT1, the main tumor glucose transporter. Indeed, GLUT1 expression was more widespread, not only in cancer cells but also in the stroma surrounding tumors of KO mice, suggesting a shift to glycolysis (Supplementary Fig. 1*E*). These data indicated that EC expression of PHB1 promotes lipid metabolism.

Endothelial Deletion of PHB1 Has No Metabolic Effect in Mice on a Low-Fat Diet

We performed a comprehensive metabolic phenotyping of PHB1 EC-KO and WT littermates. EchoMRI analysis did not reveal a difference in either fat or lean body mass accumulation in male (Fig. 2*A*) or female (Supplementary Fig. 2*A*) KO mice. There was no significant effect of PHB1 EC-KO on food consumption (Fig. 2*B*) or locomotor activity (Fig. 2*C*). Cold tolerance was unaffected in both male (Fig. 2*D*) and female (Supplementary Fig. 2*B*) KO mice. VO_2 measured by indirect calorimetry did not reveal changes in nighttime or daytime energy expenditure in KO males (Fig. 2*E*) or females (Supplementary Fig. 2*C*). There was also no significant difference detected in the respiratory exchange ratio (RER) between control and KO mice (Fig. 2*F*). There was a trend for lower nonfasting glucose levels in KO male littermates (Fig. 2*G*); however, no significant difference was detected between control and KO females (Supplementary Fig. 2*D*). GTT did not reveal a significant difference in fasting glucose clearance rates for males (Fig. 2*H*) or females (Supplementary Fig. 2*E*). Neither male (Fig. 1*I*) nor female (Supplementary Fig. 2*F*) KO mice displayed a significant difference in insulin tolerance compared with controls when raised on chow.

Mice With PHB1 Endothelial Deletion Increase Glucose Utilization on HFD

Because PHB1 has been shown to stimulate CD36-mediated LCFA transport, we also phenotyped mice after HFD feeding for 3 months, which resulted in modest fat mass gain in both WT and EC-KO mice (Supplementary Fig. 3*A*). There was no significant effect of PHB1 EC-KO on food consumption (Fig. 3*A*) or locomotor activity (Fig. 3*B*) in males. HFD-fed females also did not display a change in these parameters (Supplementary Fig. 3*B* and *C*). Cold tolerance was not significantly different in KO littermates fed the HFD (Fig. 3*C*). Indirect calorimetry did not reveal significant differences in VO_2 in KO males (Fig. 3*D*) or females (Supplementary Fig. 3*D*). However, unlike for chow feeding, the RER was elevated in both KO males (Fig. 3*E*) and females (Supplementary Fig. 3*D*). In addition, GTT revealed significantly faster glucose clearance rates for both KO males (Fig. 3*F*) and females (Supplementary Fig. 3*E*). Also, ITT revealed a higher insulin sensitivity in male (Fig. 3*G*) and female (Supplementary Fig. 3*F*) KO mice. To determine whether this phenotype is due to PHB1 EC-KO resulting in increased glucose utilization, we measured GLUT expression. Expression of GLUT4, the main adipocyte GLUT, was notably higher in both VAT and SAT of KO mice (Supplementary Fig. 3*G*). Moreover, an apparent GLUT1

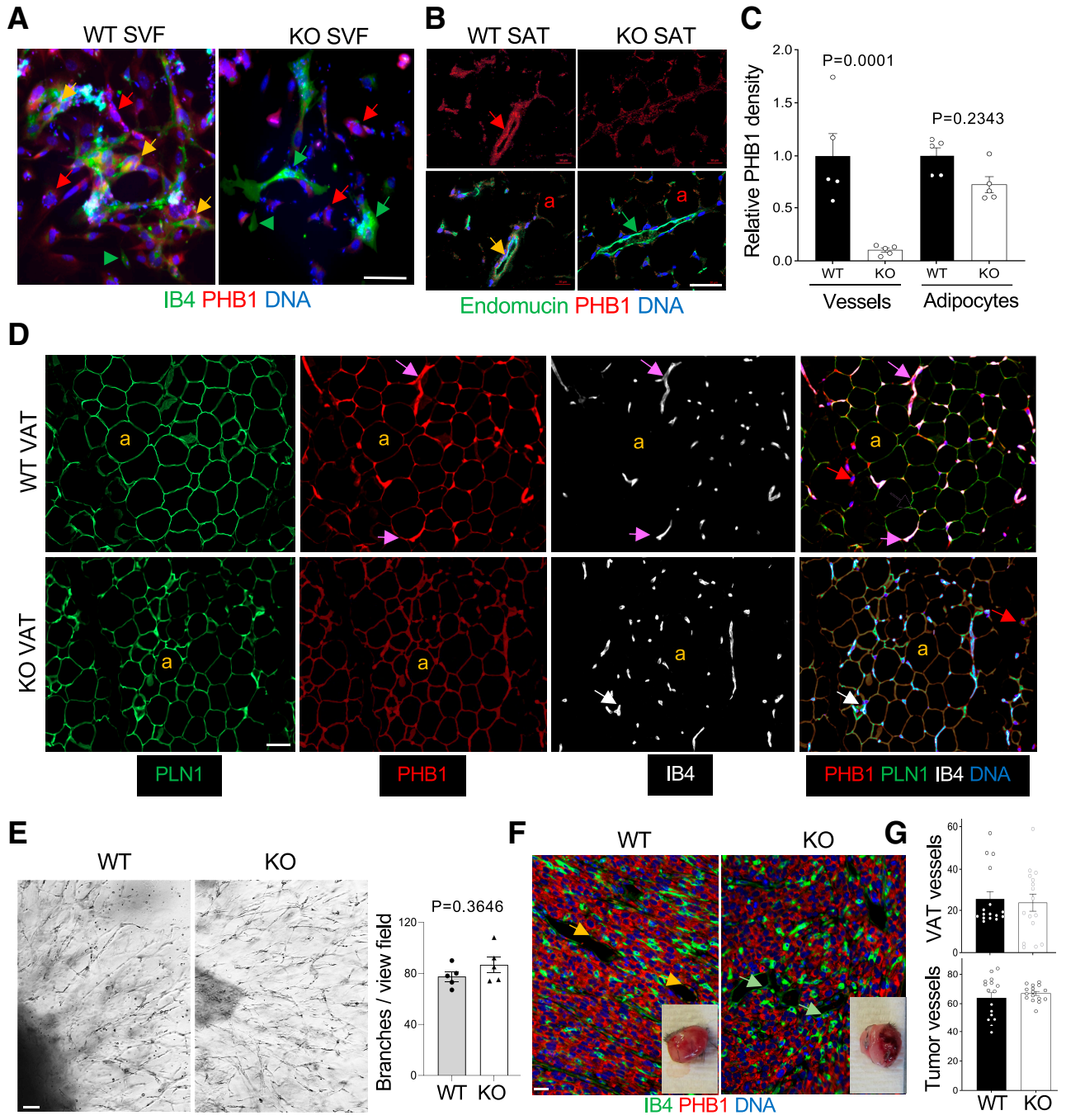

Figure 1—PHB1 EC-KO mice have normal AT and vascularization. *A:* IF of AT-derived SVF plated in culture. ECs, bound by isolectin B4 (IB4) are PHB1$^+$ in WT mice (yellow arrows) and PHB1$^-$ in KO mice (green arrows). Arrowhead: IB4$^+$ monocyte. Red arrows: stromal cells PHB1$^+$ in both WT and KO mice. *B:* IF on SAT sections reveals a lack of PHB1 in endomucin+ endothelium of KO mice (yellow arrow: colocalization in WT mice); a: PHB1$^+$ adipocytes. Quantification of PHB1 signal in IB4+ endothelium (*C*) and in perilipin-1 (PLN1)$^+$ adipocytes (*D*) by ImageJ in IF images. *P* value by Student *t* test. *D:* IF on VAT sections reveals the lack of PHB1 in IB4$^+$ endothelium (purple vs. white arrows); a: PLN1$^+$ adipocytes, which still express PHB1 in KO mice. *E:* AT explant assay showing that angiogenic sprouting is comparable for WT and PHB1 KO-ECs. Graph: branches/view field in (*E*) quantified by ImageJ. *P* value: Student *t* test. *F:* Sections of RM1 tumors grown subcutaneously subjected to anti-PHB1 IF show comparable vascular networks stained with IB4 and the lack of PHB1 in ECs of KO mice. Inset images: representative tumors upon resection. *G:* Quantification of IB4$^+$ vessel density in VAT of mice fed the HFD for 3 months and in tumors (IF images in *F* by ImageJ). In all mouse experiments, 15-month-old males ($n > 3$) were used. In all panels, scale bar: 50 μm.

upregulation was observed for the liver of KO mice (Supplementary Fig. 3*H*). After 3 months of HFD feeding, a higher proportion of adipocytes in VAT and BAT of KO mice contained smaller lipid droplets (Fig. 3*H*). Combined, these observations indicated that endothelial PHB1 plays a role in the lipid/glucose metabolism balance.

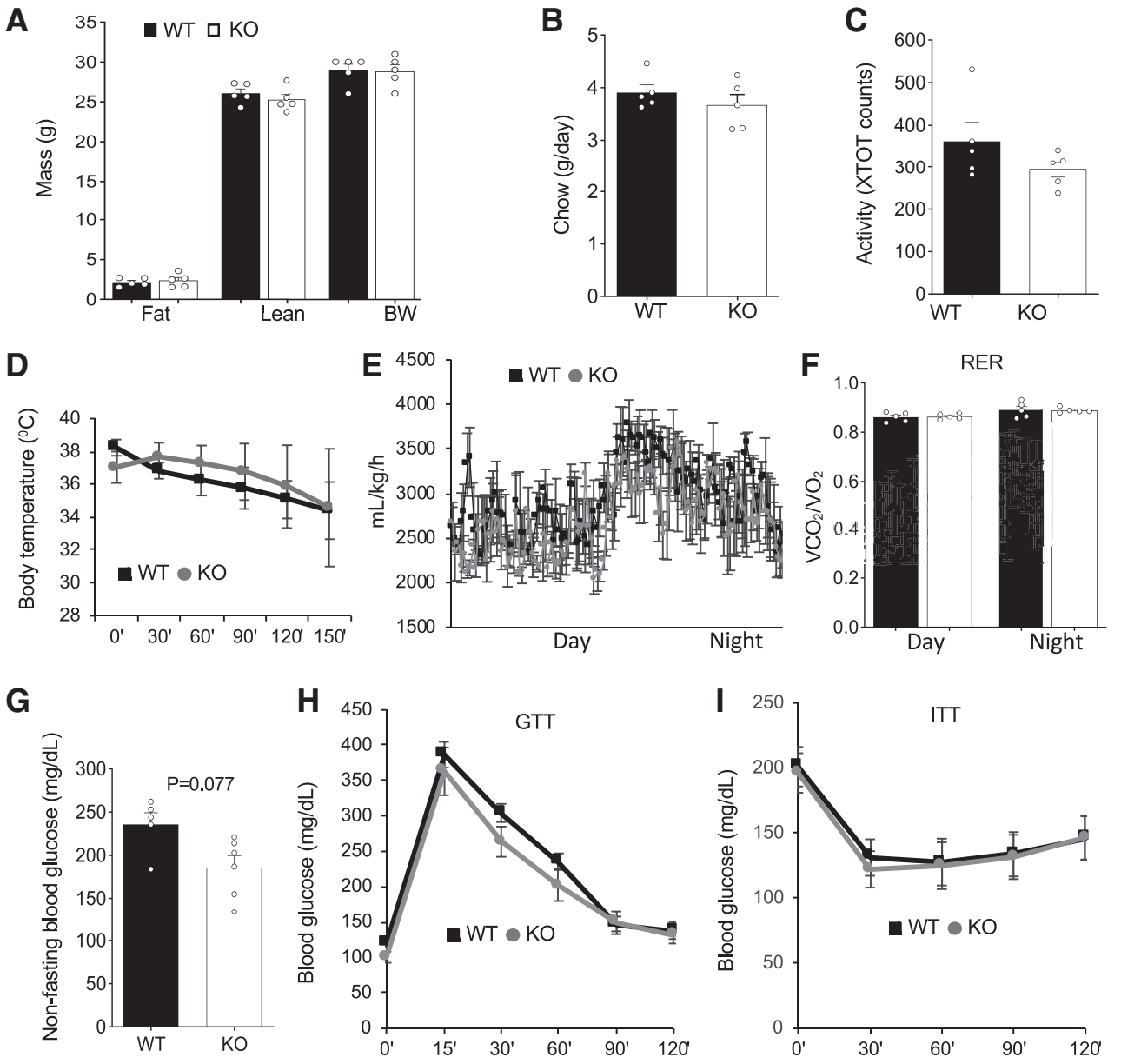

Figure 2—PHB1 EC-KO mice have no metabolic phenotype on low-fat diet. For all panels, WT and PHB1 EC-KO male littermates (n = 5) were analyzed at 16 weeks of age *A:* EchoMRI analysis reveals no difference. *B:* Chow consumption is similar. *C:* Spontaneous locomotor activity is similar. XTOT, total number of x-axis infrared-beam breaks. *D:* Body temperature maintenance in mice placed at 4°C is similar. *E:* VO_2 measured by indirect calorimetry is similar. *F:* RER (RER = VCO_2/VO_2) is similar. *G:* Nonfasting glucose concentration in blood. *H:* GTT: After overnight fasting, mice were injected with glucose (2 g/kg body wt) i.p., and glucose in blood was measured. *H:* ITT: After 4-h fasting, mice were injected with insulin (0.6 units/kg body wt) i.p., and glucose in blood was measured. In all panels, plotted data are mean ± SEM.

Lipid Metabolism Suppression in Mice With PHB1 Endothelial Deletion

To investigate the importance of endothelial PHB1 for lipid metabolism, we analyzed 8-month-old chow-fed WT and KO littermates that had no difference in body composition. Both fasting and nonfasting TAG were found to be higher in circulation of EC-KO mice (Fig. 4*A*), a phenotype previously reported for mice with defective LCFA transport (19). EC-KO mice raised on the HFD were found to have signs of hepatosteatosis, further indicating dyslipidemia (Supplementary Fig. 4*A*). Increased hepatocyte expression of HADHA, a marker of liver FAO into ketone bodies (18) indicated that FAO is activated to counter the circulating lipid overload (Supplementary Fig. 4*B*). Normal TAG content in the feces of KO mice ruled out a possibility that the phenotype results from a change in lipid assimilation

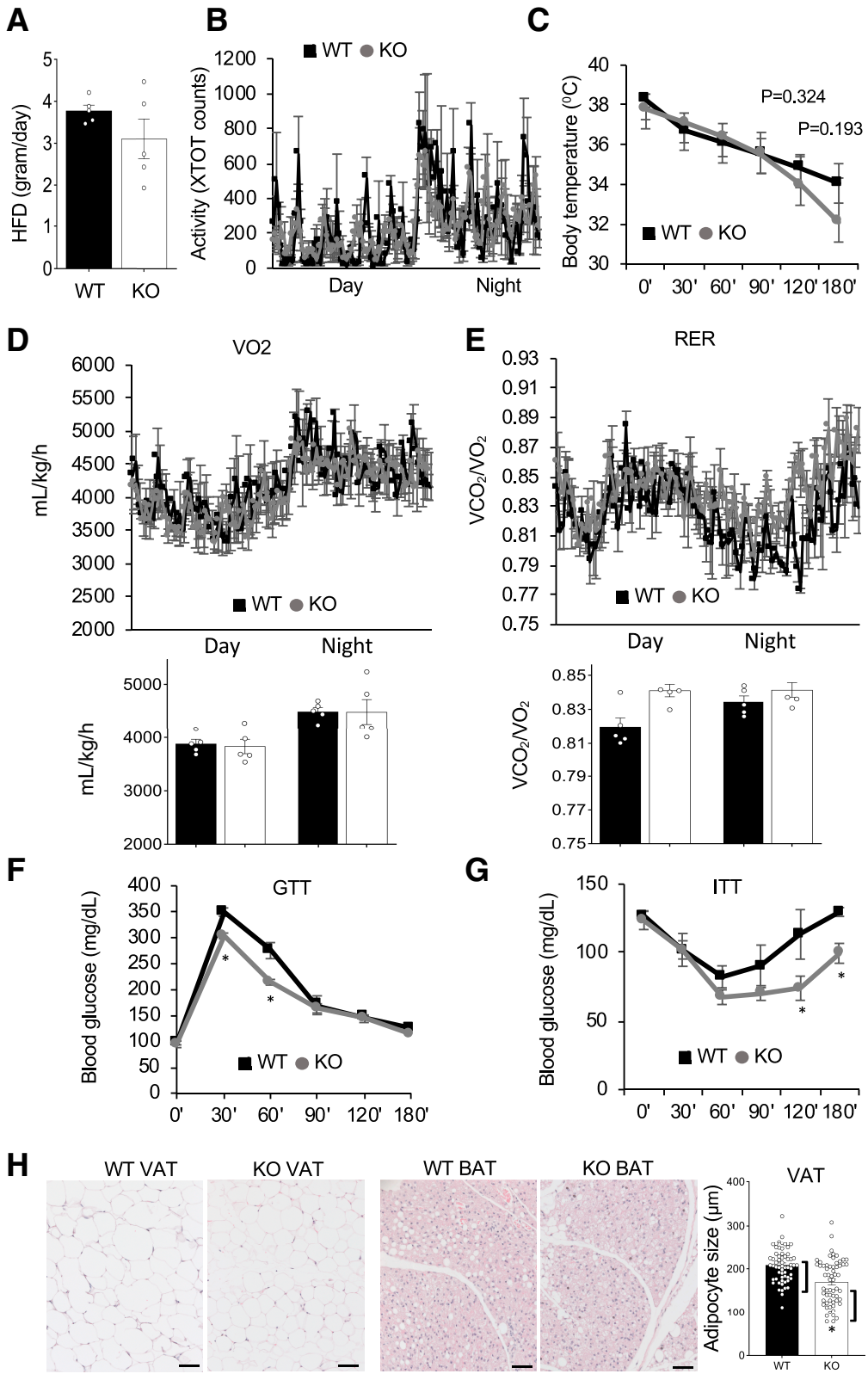

Figure 3—PHB1 EC-KO mice have a metabolic phenotype on HFD. For all panels, WT and PHB1 EC-KO male littermates ($n = 5$) were analyzed at 62 weeks of age after 3 months on the HFD. *A:* HFD consumption is similar. *B:* Spontaneous locomotor activity is similar. XTOT, total number of *x*-axis infrared-beam breaks. *C:* Cold tolerance in mice placed at 4°C. *D:* VO_2 consumption measured by indirect calorimetry with average night and day VO_2 plotted below. *E:* RER (VCO_2/VO_2) with average night and day plots below showing a significant increase. *F:* GTT in overnight fasted mice. *G:* ITT in 4 h-fasted mice. *H:* Hematoxylin and eosin staining of VAT and BAT. Graph: Quantification of adipocyte size in *H* by ImageJ. In all panels, scale bar: 50 μm. Plotted data are mean ± SEM. *$P < 0.05$ (Student *t* test).

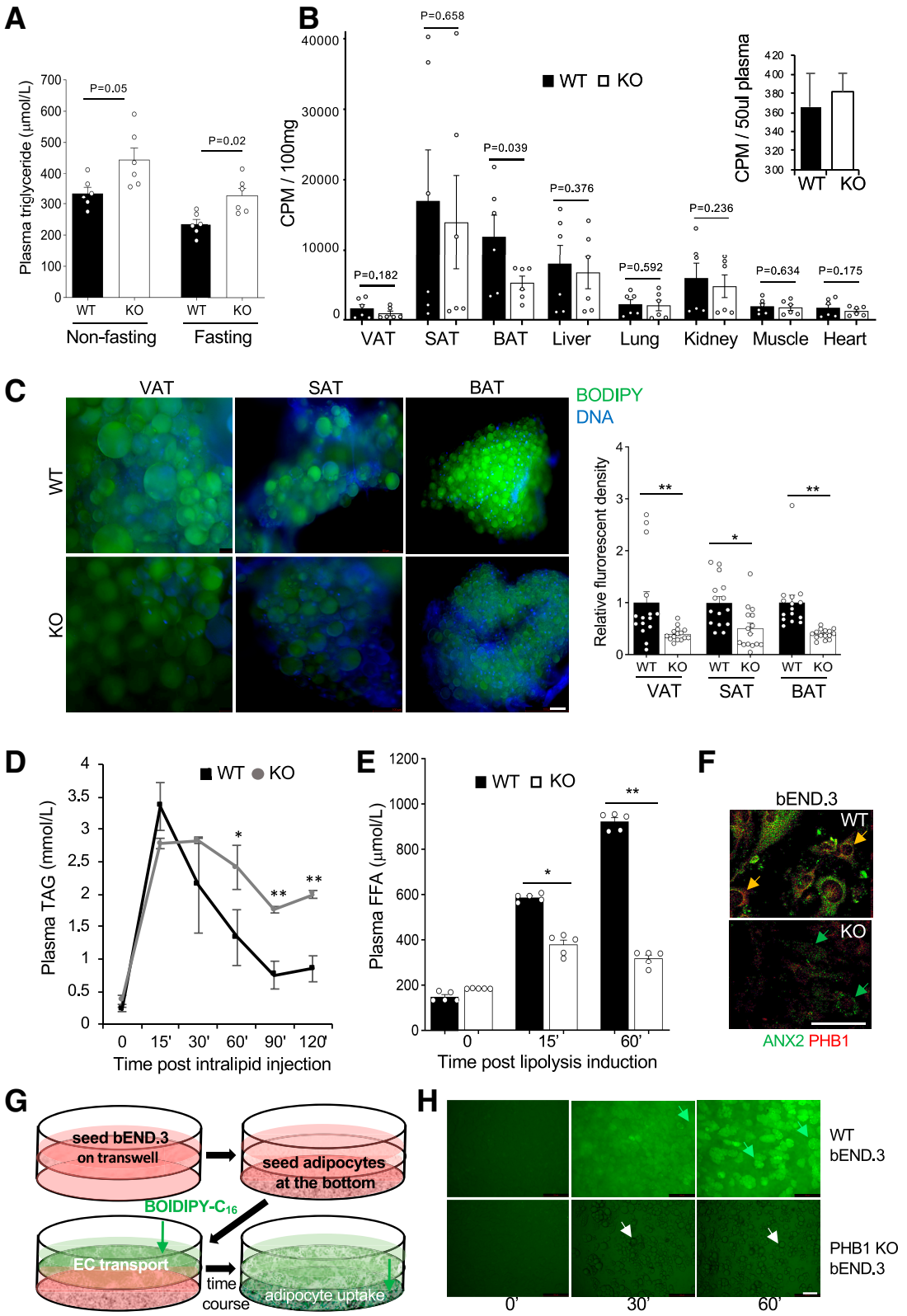

Figure 4—Lipid metabolism suppression in PHB1 EC-KO mice. *A*: Plasma TAG concentration in circulation in overnight fasted and non-fasted males ($n = 3$). *B*: In vivo LCFA uptake: data combined from two independent experiments. Upon iv administration of [^{3}H]palmitate after 30 min of circulation and subsequent perfusion to clear [^{3}H]palmitate in circulation, liquid scintillation counts per minute (CPM) were measured on indicated resected tissues. Inset: [^{3}H]palmitate in blood prior to perfusion. *C:* BODIPY-C_{16} uptake by VAT, SAT, and BAT adipocytes in WT and KO mice 3 h after iv injection. Green fluorescence was imaged in cell suspension upon tissue digestion with collagenase. Graph: Quantification of BODIPY-C_{16} signal in (*C*) by ImageJ. *D:* TAG blood concentration analysis upon iv intralipid infusion into prestarved mice shows a delay in clearance for KO littermates compared with WT. *$P < 0.05$, **$P < 0.01$ (Student *t* test). *E:* Plasma

(Supplementary Fig. 4*C*). Expression of lipoprotein lipase (LPL), which releases FA from circulating triglycerides, was also not affected in AT of EC-KO mice (Supplementary Fig. 4*D*).

To investigate the uptake of circulating LCFA, we performed liquid scintillation counting 30 min after iv administration of radiolabeled [9,10-^{3}H]palmitic acid ([^{3}H]palmitate). Equal administration into PHB1 EC-KO and WT mice was confirmed by measuring circulating [^{3}H]palmitate (Fig. 4*B*). Short term palmitate uptake was significantly lower in BAT of KO mice (Fig. 4*B*). SAT data were variable possibly due to heterogeneity of beige AT presence in samples with high palmitate uptake. In VAT, known to have relatively slow LCFA uptake rate, the ^{3}H signal was at the background level observed for control tissues (lung and muscle); in liver and kidney, the ^{3}H signal was undistinguishable between KO and WT mice (Fig. 4*B*). To assess the importance of EC PHB1 over a longer period of time, we iv injected mice with a fluorophore-labeled palmitic acid, BODIPY-FL-C_{16}, and analyzed AT recovered after 180 min of circulation. BODIPY-FL-C_{16} accumulation was significantly lower in adipocytes of PHB1 EC-KO mice compared with WT controls, with the difference again particularly striking for BAT (Fig. 4*C*). This was not due to an intrinsic adipocyte change, as adipocytes from KO mice differentiated in culture were found to uptake LCFA normally (Supplementary Fig. 4*E*). These data indicated that endothelial PHB1 is specifically important for LCFA uptake in AT. The defect in LCFA assimilation was also confirmed by a lipid tolerance test. Upon intralipid infusion, the time course of triglyceride blood concentration demonstrated delayed LCFA clearance for PHB1 EC-KO littermates compared with WT (Fig. 4*D*). We also investigated the importance of endothelial PHB1 for the release of lipids from AT. Upon lipolysis induction by the β-adrenergic agonist isoproterenol, circulating FFA levels were expectedly increased. Compared with WT mice, FFA mobilization was significantly blunted in PHB1 EC-KO littermates (Fig. 4*E*). Hormone-sensitive lipase phosphorylation in adipocytes from PHB1 EC-KO and WT mice was undistinguishable upon isoproterenol treatment, indicating that that lipolysis in adipocytes is normal and does not account for the phenotype (Supplementary Fig. 4*F*).

To directly examine a role of PHB1 in LCFA transport across the endothelium, we used a mouse bEND.3 endothelial cell line. PHB1 was knocked out by using the clustered regularly interspaced short palindromic repeats (CRISPR)/Cas9 method (Supplementary Fig. 4*G*). Interestingly, expression of ANX2, a protein found in complex with PHB1 and CD36 (8), was downregulated in PHB1-KO cells (Fig. 4*F*). Analysis of AT expression by IF provided further evidence for endothelial ANX2 downregulation in the absence of PHB1 (Supplementary Fig. 4*H*). We then developed an assay measuring LCFA transport across the endothelium (Fig. 4*G*). To simulate the endothelial wall lining, we seeded a monolayer of WT or KO bEND.3 cells on a transwell. WT adipocytes seeded in the lower chamber were used to read out BODIPY-FL-C_{16} transport. BODIPY-FL-C_{16} added into the upper chamber was transported across bEND.3 cells and deposited into adipocyte lipid droplets in a time-dependent manner (Fig. 4*H*). In contrast, no transport was observed across KO bEND.3 cells, as evident from a complete lack of BODIPY-FL-C_{16} deposition in adipocytes (Fig. 4*H*). Combined, our results indicate the importance of endothelial PHB1 for bidirectional LCFA transport in AT.

DISCUSSION

Our study shows that PHB1 in ECs regulates LCFA transport in AT, suppression of which results in reduced LCFA utilization and increased glucose utilization as an energy source in both male and female mice. Interestingly, the phenotype of PHB1 EC-KO mice is starkly different from that of PHB1 adipocyte-KO mice reported previously (7). While PHB loss in adipocytes also resulted in reduced LCFA transport in AT and increased glucose utilization, PHB1 adipocyte-KO mice have hyperplastic adipocytes and are insulin resistant (7). As we have demonstrated, T2D development in PHB1 adipocyte-KO mice is largely due to defects in adipocyte mitochondrial oxidation dysfunction, lipolysis, and adaptive thermogenesis. It is not surprising that these processes are not affected in PHB1 EC-KO mice.

Our results demonstrate that endothelial deletion of PHB1 does not affect vascularization of AT in development and that its function in ECs is dispensable for angiogenesis. This suggests that intracellular PHB1 function in the endothelium is not critical. The phenotype of EC-KO mice clearly indicates the role of PHB1 in lipid metabolism. Intestinal lipid absorption and indirect changes in adipocytes we ruled out here as possible mechanisms of endothelial PHB1 function. The stimulation of LCFA transport in AT appears to be the main role of PHB1 in the endothelium. It is likely that this function is linked with the cell-surface PHB1 localization in AT endothelium reported previously (9), which is consistent with the lack of endothelial PHB1 deletion effect in other organs. LCFA transport is mediated first by LPL, then

concentration of FFA after isoproterenol injection increases less in KO mice than in WT. *A–E*: Experiment used 8-month-old males raised on chow. *F:* Expression of PHB1 and ANX2 in b.END3 cells (parental and PHB1-KO) detected by IF. *G:* Schematic of the assay (*H*) measuring LCFA transport across a monolayer of bEND.3 endothelial cells. *H:* WT and PHB1-KO bEND.3 were grown to 100% confluency on the top of the 0.4-μm pore transwells; adipocytes differentiated from WT MEFs were seeded in the bottom of the wells. BODIPY-C_{16} (2 μmol/L) was added to the upper chamber, and then adipocytes in the lower chamber were imaged after the time indicated. LCFAs are transported through control bEND.3 cells and deposited into adipocytes (green arrows), PHB1-KO bEND.3 cells do not transport LCFAs into adipocytes (white arrows). In all panels, data plotted are mean ± SEM. *$P < 0.05$, **$P < 0.01$ (Student *t* test). Scale bar: 50 μm.

by CD36, and subsequently by the FA transport proteins (FATPs). According to our expression analysis, LPL function, particularly important in ECs, does not appear to be affected in PHB1-KO mice. Because PHB1 is not known to interact with FATPs, the main mechanism of PHB1 action appears to be assisting CD36, along with ANX2 (13). Consistent with this, the phenotype observed here is similar to those reported for mice with endothelial KO of CD36 (20) and for ANX2-KO mice (8). Interestingly, downregulation of ANX2, a protein found in complex with PHB1 and CD36, in PHB1-KO cells (Fig. 4*F*) is consistent with PHB1 downregulation previously reported for ANX2-KO (8). For endothelial KO of CD36, LCFA uptake defect was observed in AT as well as skeletal muscle, but not in liver (20). Because PHB1 is selectively displayed on the surface of ECs in AT, but not in skeletal muscle or liver, it is unlikely that PHB1 EC-KO in those organs directly contributes to the phenotype we report, which is consistent with normal LCFA uptake in liver and muscle (Fig. 4*B*). However, EC PHB1 loss in organs other than AT may still contribute to lipid metabolism regulation.

The question regarding cell surface versus intracellular role of PHB1 in ECs remains open. To attempt addressing it, we injected mice with phage-displayed KGGRAKD, a peptide binding to cell membrane-expressed PHB1 in AT (9). As expected, KGGRAKD homed to SAT vasculature in WT but not in PHB1 EC-KO mice (Supplementary Fig. 5*A* and *B*). Because adipocytes also express PHB1 on the surface, the lack of KGGRAKD localization in adipocytes of KO mice indicates that endothelial PHB1 is required for peptide transport across the endothelium, as it is for LCFA transport. Interestingly, KGGRAKD-phage homing to BAT was not observed in either WT or KO mice, which was confirmed by IF (Supplementary Fig. 5*A* and *B*). Because our study clearly shows that endothelial PHB1 is important for LCFA transport in BAT, this is a surprising result. A possible explanation is that PHB1 protein interactions and/or folding in the cell membrane of BAT endothelium is different from that in SAT and is incompatible with the peptide binding. Alternatively, in BAT endothelium, PHB1 may be not localized to the surface and may facilitate LCFA trafficking through a mechanism distinct from that in WAT.

The new data from this study are important in considering PHB1 as a drug target. A proapoptotic peptide (Adipotide), directed with KGGRAKD to endothelial PHB1, has been shown to deplete AT ECs and reverse obesity in various animal models (9,21,22). Our study further validates the WAT vascular-targeting capacity of KGGRAKD peptide and offers PHB1 EC-KO mice as a tool that could be used to assess possible off-target effects of Adipotide. Small molecules interfering with PHB1 function have been characterized previously (2) and proven potent to block LCFA utilization and increase glucose utilization by adipocytes (7). This study demonstrates that PHB1 inactivation in ECs also contributes to this metabolic switch. While PHB1 inactivation in brown adipocytes has adverse metabolic consequences due to inhibition of nonshivering thermogenesis, it could be possible to dose or formulate systemically administered PHB1 inhibitors to only block its function in ECs. The potential usefulness of PHB1 as a drug target remains to be determined.

Acknowledgments. The authors thank Shelly Lu (Cedars-Sinai Medical Center) for providing $Phb1^{fl/fl}$ mice.

Funding. This work was supported by National Institutes of Health National Institute of Diabetes and Digestive and Kidney Diseases grant 2R01DK088131 to M.G.K., the Bovay Foundation, and the Levy-Longenbaugh Fund.

Duality of Interest. No potential conflicts of interest relevant to this article were reported.

Authors Contributions. Z.G., A.C.D., and Y.Y. designed and performed the experiments, analyzed data, and edited the manuscript. Z.G. and M.G.K. conceived and designed the experiments, analyzed data, and wrote the manuscript. M.G.K. is the guarantor of this work and, as such, had full access to all the data in the study and takes responsibility for the integrity of the data and the accuracy of the data.

References

1. Ande SR, Nguyen KH, Nyomba BLG, Mishra S. Prohibitin in adipose and immune functions. Trends Endocrinol Metab 2016;27:531–541

2. Wang D, Tabti R, Elderwish S, et al. Prohibitin ligands: a growing armamentarium to tackle cancers, osteoporosis, inflammatory, cardiac and neurological diseases. Cell Mol Life Sci 2020;77:3525–3546

3. Ande SR, Nguyen KH, Padilla-Meier GP, Wahida W, Nyomba BL, Mishra S. Prohibitin overexpression in adipocytes induces mitochondrial biogenesis, leads to obesity development, and affects glucose homeostasis in a sex-specific manner. Diabetes 2014;63:3734–3741

4. Zhang F, Hao G, Shao M, et al. An adipose tissue atlas: an image-guided identification of human-like BAT and beige depots in rodents. Cell Metab 2018;27:252–262.e3

5. Sun K, Tordjman J, Clément K, Scherer PE. Fibrosis and adipose tissue dysfunction. Cell Metab 2013;18:470–477

6. Kajimura S, Spiegelman BM, Seale P. Brown and beige fat: physiological roles beyond heat generation. Cell Metab 2015;22:546–559

7. Gao Z, Daquinag AC, Fussell C, Djehal A, Désaubry L, Kolonin MG. Prohibitin inactivation in adipocytes results in reduced lipid metabolism and adaptive thermogenesis impairment. Diabetes 2021;70:2204–2212

8. Salameh A, Daquinag AC, Staquicini DI, et al. Prohibitin/annexin 2 interaction regulates fatty acid transport in adipose tissue. JCI Insight 2016;1:e86351

9. Kolonin MG, Saha PK, Chan L, Pasqualini R, Arap W. Reversal of obesity by targeted ablation of adipose tissue. Nat Med 2004;10:625–632

10. Staquicini FI, Cardó-Vila M, Kolonin MG, et al. Vascular ligand-receptor mapping by direct combinatorial selection in cancer patients. Proc Natl Acad Sci U S A 2011;108:18637–18642

11. Ko KS, Tomasi ML, Iglesias-Ara A, et al. Liver-specific deletion of prohibitin 1 results in spontaneous liver injury, fibrosis, and hepatocellular carcinoma in mice. Hepatology 2010;52:2096–2108

12. Kano A, Wolfgang MJ, Gao Q, et al. Endothelial cells require STAT3 for protection against endotoxin-induced inflammation. J Exp Med 2003;198:1517–1525

13. Daquinag AC, Gao Z, Fussell C, et al. Fatty acid mobilization from adipose tissue is mediated by CD36 posttranslational modifications and intracellular trafficking. JCI Insight 2021;6:e147057
14. Gao Z, Daquinag AC, Fussell C, et al. Age-associated telomere attrition in adipocyte progenitors predisposes to metabolic disease. Nat Metab 2020;2:1482–1497
15. Goudriaan JR, den Boer MA, Rensen PC, et al. CD36 deficiency in mice impairs lipoprotein lipase-mediated triglyceride clearance. J Lipid Res 2005;46:2175–2181
16. Lenz LS, Marx J, Chamulitrat W, et al. Adipocyte-specific inactivation of Acyl-CoA synthetase fatty acid transport protein 4 (Fatp4) in mice causes adipose hypertrophy and alterations in metabolism of complex lipids under high fat diet. J Biol Chem 2011;286:35578–35587
17. Min SY, Kady J, Nam M, et al. Human 'brite/beige' adipocytes develop from capillary networks, and their implantation improves metabolic homeostasis in mice. Nat Med 2016;22:312–318
18. Pan A, Sun XM, Huang FQ, et al. The mitochondrial β-oxidation enzyme HADHA restrains hepatic glucagon response by promoting β-hydroxybutyrate production. Nat Commun 2022;13:386
19. Daquinag AC, Gao Z, Fussell C, et al. Fatty acid mobilization from adipose tissue is mediated by CD36 post-translational modifications and intracellular trafficking. JCI Insight 2021;6:e147057
20. Son NH, Basu D, Samovski D, et al. Endothelial cell CD36 optimizes tissue fatty acid uptake. J Clin Invest 2018;128:4329–4342
21. Barnhart KF, Christianson DR, Hanley PW, et al. A peptidomimetic targeting white fat causes weight loss and improved insulin resistance in obese monkeys. Sci Transl Med 2011;3:108ra112
22. Kim DH, Woods SC, Seeley RJ. Peptide designed to elicit apoptosis in adipose tissue endothelium reduces food intake and body weight. Diabetes 2010;59:907–915